

Influences of the pre-chamber orifices on the combustion behavior in a constant volume chamber simulating pre-chamber type medium-speed gas engines

ARTICLE INFO

Received: 12 February 2022
Revised: 19 March 2022
Accepted: 8 April 2022
Available online: 17 April 2022

The study aims to clarify the influence of pre-chamber (PC) configurations on the combustion process in the main chamber (MC) of medium-speed spark-ignition gas engines equipped with an active PC. A constant volume combustion chamber was prepared to simulate the chamber configurations of the gas engines. A high-speed shadowgraph was applied to visualize the torch flame development and the combustion process in the MC. Experiments were done by changing the charged gas in the MC, the number, and the diameter of the PC orifices. Combustion was most accelerated when the PC orifice configuration was set appropriately so that the adjacent torch flames would combine with each other. It was also found that the unburned mixture in the PC, which ejected prior to the torch flame, supported the penetration of the torch flame.

Key words: gas engine, pre-chamber, torch flame, combustion visualization, natural gas

This is an open access article under the CC BY license (<http://creativecommons.org/licenses/by/4.0/>)

1. Introduction

In recent years, emission regulations on internal combustion engines have become stricter because of global environmental issues growing concern. Harmful emissions such as NO_x, SO_x, and PM have long been regulated due to their direct impact on human health, and GHG reduction is now an urgent issue. Then natural gas has become popular in marine and industrial applications because it emits less carbon dioxide, no sulfur, and much fewer PM [1]. Moreover, natural gas is so flexible that it can be used in both diffused combustion (gas diesel) and premixed combustion (gas engine). Except for extra-large propulsion applications, premixed gas engines are used regularly. In premixed combustion of natural gas, a lean combustion system reduces fuel consumption, reduces thermal NO_x, and improves thermal efficiency [2]. However, a leaner mixture has less ignitability and lower combustion speed [3], and it tends to result in methane slippage [4] and cycle to cycle variation [5, 6]. Hence, various high-energy ignition methods are necessary, such as plasma ignition [7–9], laser-induced ignition [10], and pre-chamber (PC) ignition [11].

A combustion chamber is separated into two different chambers in the PC ignition gas engines. One is the main chamber (MC), surrounded by a cylinder head, cylinder liner, and piston. Another is a pre-chamber with a small volume of around 2% of the MC and is connected to the MC through its multiple orifices. Firstly, a spark plug ignites the mixture in the PC, and then a hot flame propagates in the PC. Finally, flame jets eject through the orifices into the MC as enhanced ignition sources, sometimes called torch flames or turbulent jets. The PC ignition has been proved to improve the stability and reproducibility of the MC combustion and promote heat release by dispersing the ignition location and increasing ignition energy [12].

The PC ignition is divided into two types according to the method of filling the PC with the mixture: active type and passive type. The former has an independent fuel supply system, while the latter utilizes the mixture flowing

from the MC during a compression stroke. The active PC requires the additional cost of a separate mixture delivery system. Still, it has significant advantages in increasing the ignition energy of the flame jets and in expanding the lean limit of the MC mixture [13, 14].

The PC combustion system, known as turbulent jet ignition (TJI) in the automotive field, has been comprehensively and thoroughly reviewed by Alvarez et al. [15], and more recently by Zhua et al. [16]. In order to investigate the detailed mechanism of PC combustion, optical visualization of combustion using rapid compression machines (RCM) and constant volume combustion chamber (CVCC), a numerical simulation based on CFD, and experimental studies using actual metal engines have been conducted. Validi et al. [17] performed numerical simulations of combustion in a rapid compression machine (RCM) using an LES/FMDF computational model. They suggested that there are three main combustion phases for turbulent jet ignition in the RCM: (i) cold fuel jet, (ii) turbulent hot product jet, and (iii) reverse fuel-air/product jet. Sadanandan et al. [18] studied the ignition behavior of unburned hydrogen/air mixtures by combining OH-LIF, fast sequences of Schlieren images, and simple numerical simulations. From their observations, ignition was found to occur near the tip of the jet but not at the sides of the jet due to the difference in mixing behavior. Biswas et al. [19] performed simultaneous measurements of fast Schlieren and OH/chemiluminescence methods for PC combustion of premixed CH₄/air and H₂/air to visualize the process of jet penetration and ignition. They clarified the existence of two ignition mechanisms: flame ignition (ignition by reacting jet) and jet ignition (ignition by reacted jet). They also note that as the orifice diameter of the PC increases, the ignition mechanism tends to switch from jet ignition to flame ignition, with flame ignition becoming more dominant as the pressure increases.

The geometric parameters of the PC are essential factors that determine the quench of the flame through the orifice, the velocity of the jet of combustion products, the disper-

sion of the ignition point in the MC, and the turbulent structure [20, 21]. Gentz et al. [22] investigated the effects of the number of orifices and the amount of auxiliary fuel on combustion by optical observation and pressure analysis using the RCM. They showed that changing the number of orifices caused differences in end-gas autoignition behavior. Zhou et al. [23] conducted optical observations of CVCC and tests on a single-cylinder engine and showed that the adoption of an appropriate multi-orifice PC leads to improved combustion and that a smaller orifice diameter leads to jet flame quenching. However, there are few examples of investigations of the effect of PC structure on combustion, simulating engines with large bores, such as marine engines and industrial generators [24].

In this study, optical observation and pressure analysis were conducted in a CVCC with a large bore to investigate the effects of the PC orifice diameter, the number of orifices, and the main chamber gas on the torch flame ejection and the main chamber combustion.

2. Experimental methods

2.1. Constant volume combustion chamber

All experimental testing was performed in an optically accessible Constant Volume Combustion Chamber (CVCC). The schematic view and main specifications of the tested CVCC are shown in Fig. 1 and Table 1 respectively.

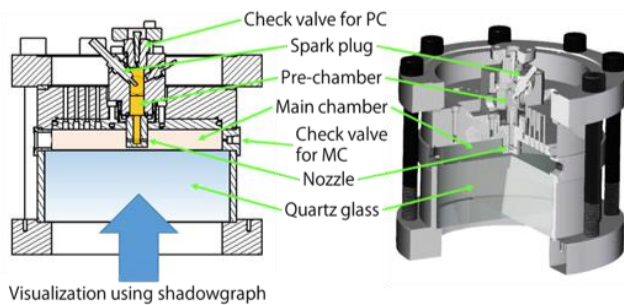


Fig. 1. Schematic of the constant volume combustion chamber (CVCC)

Table 1. Main specifications of the CVCC

Main chamber (D × H)	∅240 mm × 30 mm
Optical window (D × t)	Quartz, ∅260 mm × 100 mm
Max. pressure	10 MPa
Fuel gas in pre-chamber	CH ₄ /air premixture
Ambient gas in the main chamber	N ₂ , Air, CH ₄ /air premixture

The diameter (∅240 mm) and height (30 mm) of the tested combustion chamber correspond to the shape of the main combustion chamber at the top dead center of a typical medium-speed natural gas engine. The PC is installed above the MC, and the configurations of the PC, such as orifice diameter and the number of orifices, can be changed by exchanging the PC tip. The PC and MC have independent air/fuel mixture intake paths, and each can supply air/fuel mixture of different compositions. The bottom of the MC is made entirely of quartz glass, and the inner surface of the chamber top lid is mirror polished, allowing full optical access to in-cylinder combustion phenomena from the bottom. A pressure sensor, gas supply port for the MC, and an exhaust valve are installed on the side of the MC.

A spark plug and another pressure sensor are inserted at an angle from the side of the PC. The gas supply port for the PC locates at the top of the PC.

2.2. PC tip configuration

The experiments of the study were done by exchanging PC tips and using the main body of the PC in common. Figure 2 and Table 2 show the cross-sectional view of the PC tip and the list of PC specifications. Five PC tips identified as #1~#5 were prepared to explore the effect of PC configuration on the combustion process. The PC orifices were drilled horizontally to measure the cone angle and penetration of the torch flame directly from the visualized combustion images through the bottom window of the CVCC. The reference configuration is tip number #1, where the orifice diameter; D_{ori} is 3.5 mm and the number of orifices; N_{ori} is eight. Tips #2 and #3 have N_{ori} values of 6 and 10, respectively, and their D_{ori} is determined so that the total area of orifices is almost the same as that of #1 tip. For tips #4 and #5, N_{ori} was set constant at 8 and D_{ori} was set to 2.5 mm and 5.0 mm, respectively.

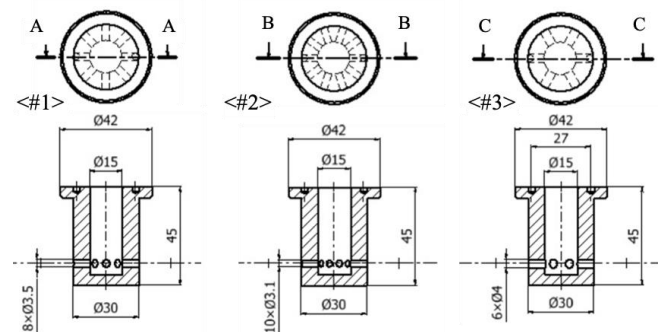


Fig. 2. Cross-sectional view of the PC tip #1~#3

2.3. Mixture preparation

As previously mentioned, the CVCC has independent gas supply systems. Figure 3 shows the schematic diagram of the gas supply systems. The supply system has a primary mixer that prepares the artificial air from O₂ and N₂, and a secondary one that prepares CH₄/Air mixture. Pressure regulators and solenoid valves are inserted in the pipeline, and the air/fuel ratio of the mixture is minutely determined by controlling the pulse duty ratio of the solenoid valves. This configuration assures the productivity of the experiments.

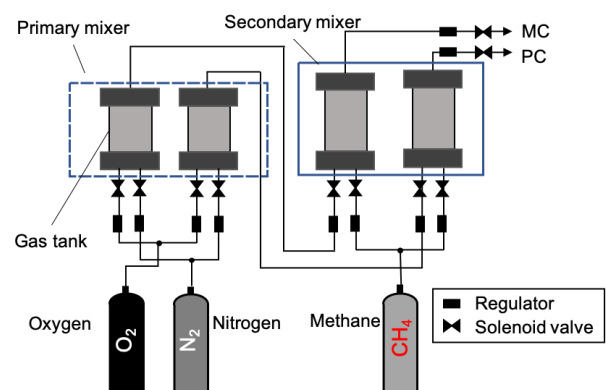


Fig. 3. Schematic of the gas supply system

Table 2. Main specifications of the pre-chamber tip #1~#5

PC tip ID	Orifice dia.: D_{ori} [mm]	Orifice length: L_{ori} [mm]	No. of orifices: N_{ori} [-]	Tip inner dia.: D_{tip} [mm]	V_{PC} ratio to V_{MC} [%]	L_{ori}/D_{ori} [-]	Area of orifices: A_{ori} [cm ²]	A_{ori} ratio to V_{PC} [cm ⁻¹]
#1	Ø3.5	7.5	8	Ø15	2.3	2.14	0.770	0.0271
#2	Ø4.0	7.5	6	Ø15	2.3	1.86	0.754	0.0265
#3	Ø3.1	7.5	10	Ø15	2.3	2.42	0.755	0.0265
#4	Ø2.5	7.5	8	Ø15	2.3	3.00	0.393	0.0138
#5	Ø5.0	7.5	8	Ø15	2.3	1.50	1.571	0.0052

Table 3 summarizes the conditions of the charging gas in the MC and PC in the experiments. Three different gases were charged as atmospheric gas in the MC. The first one is nitrogen, in which the torch flame ejected from the PC cannot continue its combustion, and the pure behavior of a torch flame can be captured. The second is artificial air, in which the torch flame can sustain its combustion by entraining oxygen in the artificial air. The third one is the lean CH₄/Air mixture, in which an entire combustion process from the ignition of the lean mixture by torch flames to the growth of ignited flame in the MC can be observed. Hereafter, these ambient gas conditions are classified as “inert”, “sustainable”, or “combustible”, respectively.

Table 3. Charging gas conditions in the main chamber and pre-chamber

Reaction in MC	“Inert”	“Sustainable”	“Combustible”
Gas in PC	CH ₄ /Air mixture ($\lambda = 1.0$)		
Gas in MC	Nitrogen	Artificial air	CH ₄ /Air ($\lambda = 1.7$)
Input heat in MC	39 kJ		
Input heat in PC	0.0 kJ	0.0 kJ	1.5 kJ
Initial pressure	1.0 MPa		
Initial temperature	290 K		

2.4. High-speed shadowgraph imaging

Figure 4 and Fig. 5 show a schematic of the shadowgraph optical setup and a detailed view of the optical path of the bottom-up optics layout in this experiment. As known, the premixed flame in gas engines is difficult to visualize, especially under lean-mixture conditions in the gas engines. The shadowgraph optical system was applied in the study. A parallel light beam is irradiated perpendicularly to the measurement volume in the technique.

Since each ray passing through the volume refracts proportional to the quadratic spatial gradient of the density, the pattern of brighter and darker spots is acquired if the disturbance of the density field caused by premixed flame exists in the measurement volume. In the experiment, double path type shadowgraph optics was realized thanks to the mirror-polished chamber lid and bottom-up optics layout, and the half mirror between a shadowgraph light source and a high-speed camera. The high-speed CMOS camera (Photron Ltd., SA-Z) with Nikon Teleconverter TC200 2X and Nikon f 2.8 objective lenses were used to take shadowgraph images of torch flame and combustion process in the MC. The frame rate was set to 20,000 fps, and the shutter speed was set to 10.0 μ s. The camera resolution was set to 1024 × 1024 pixels. An argon ion laser (Spectra-Physics, Inc., Stabilite 2017) was prepared as a light source. Another high-speed camera (Photron Ltd., SA4) was applied to determine the ignition timing of the spark plug in the PC.

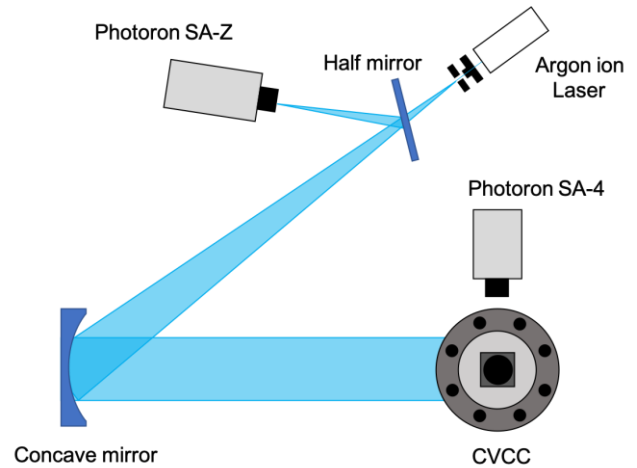


Fig. 4. Bird's eye view of the shadowgraph optical setup

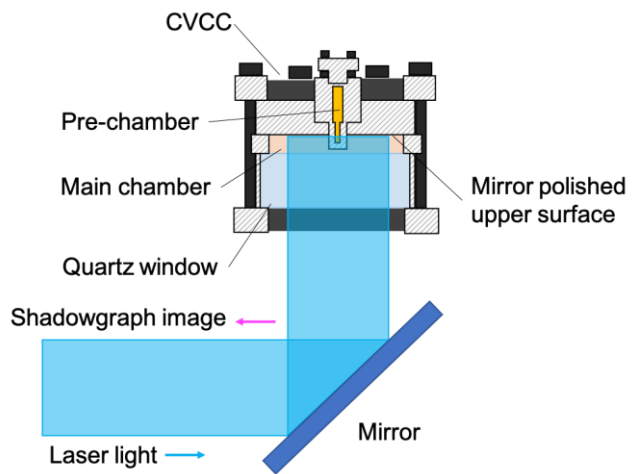


Fig. 5. Detailed view of the double path type shadowgraph optics and the bottom-up optical layout

3. Results and discussion

3.1. Effects of the main chamber atmosphere

As listed in Table 3, three different gases were charged as ambient gas in the MC. Figure 6 shows an example of torch flame observation in the MC. The figure also exemplifies the definition of penetration and cone angle. The former is the distance from the orifice exit to the tip of a torch flame. It should be noted that the penetration is determined based on a clear boundary formed by the flame front. The latter is quantified as the angle between two tangent lines descending from the center of the PC to the outer edge of the torch flame.

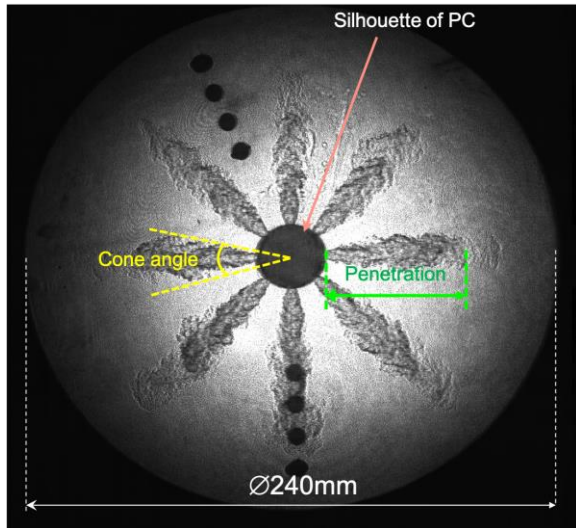


Fig. 6. Example of torch flame observation in the main-chamber

Figure 7 shows the time history of penetration and cone angle of the torch flames under the three different ambient gas conditions, and Fig. 8 shows the shadowgraph images of the torch flames corresponding to the above conditions. The elapsing time in Fig. 7 starts when the torch flames begin ejecting from the orifices of the PC. The experiments were conducted five times for all the conditions, and the penetration and the cone angle of the torch flame are obtained as the averages of the torch flames from all orifices, and furthermore, they are averaged over the five runs.

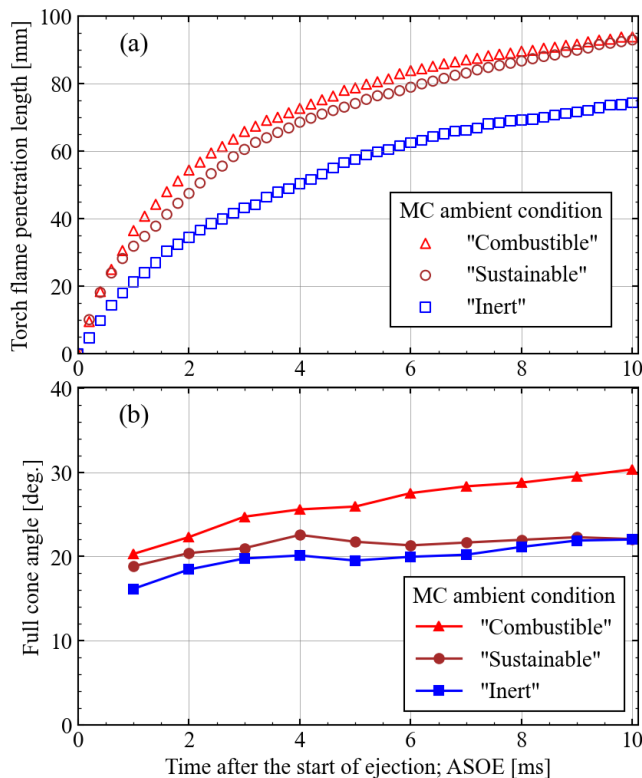


Fig. 7. Time history of (a) penetration, and (b) cone angle of torch flames under different main chamber gas conditions; “combustible” (lean CH_4/air mixture), “sustainable” (artificial air), and “inert” (N_2)

Validi et al. [9] pointed out that the unburned mixture in the PC was forced out into the MC ahead of the torch flame. This unburned mixture ejection significantly influences the torch flame behavior in the MC. The unburned mixture entrains the MC ambient gas along with the progression of the torch flame. When the unburned mixture on the tip of the torch flame is diluted by the nitrogen, the penetration becomes much shorter than in the other two (“sustainable”, “combustible”) cases.

The penetration in the “sustainable” case is almost equal to the “combustible” case at 10 ms ASOE (after the start of ejection) despite the slight shortness in the early stage of the ejection. In the “sustainable” case, the penetration comparable with the “combustible” case is hard to be expected since the torch flames barely maintain the thermal reactions. These findings could be explained as follows. The unburned tip keeps combustible by entraining fresh air, and it can contribute to maintaining the apparent flame length.

Contrarily, the cone angle of the torch flame varies significantly depending on the combustibility of the MC gas. In both the “inert” and “sustainable” cases, the cone angle remained at around 20 degrees during the entire development process of the torch flame. In contrast, that in the “combustible” case was consistently more extensive than the other two and increased monotonically with time, reaching about 30 degrees at 10 ms ASOE.

These results indicate that the flame propagation of the MC occurs mainly in the direction perpendicular to the torch flame axis, not parallel to the axis.

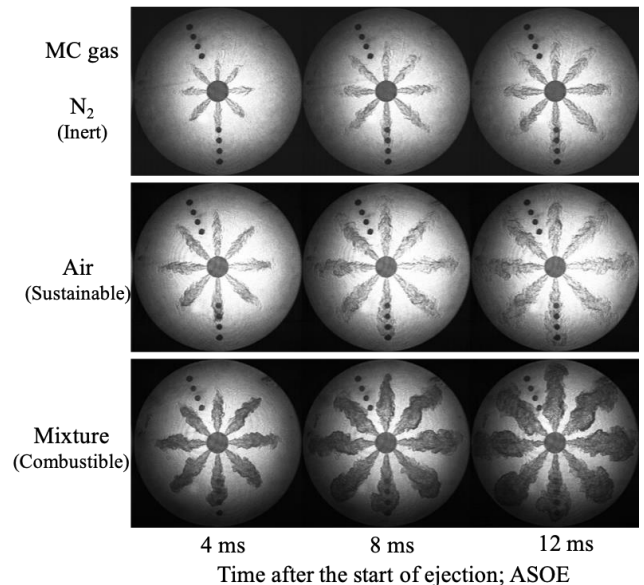


Fig. 8. Shadowgraphs of torch flames under different main chamber gas conditions; “combustible” (lean CH_4/air mixture), “sustainable” (artificial air), and “inert” (N_2)

3.2. Effects of the number of orifices

In this section, the effects of the number of orifices (N_{ori}) of the PC on torch flame and combustion are explored based on the visualization and pressure analysis. Similar to the number of nozzles in a compression ignition engine, the number of orifices in a PC-type gas engine is an important design factor that directly impacts the flame distribution and the contact area with the MC mixture. The

number of orifices (N_{ori}) in the study was selected to be 6, 8, and 10 (tip ID #1, #2, and #3). The PC volume was constant regardless of the number of the orifices. The orifice diameters were 4.0 mm, 3.5 mm, and 3.1 mm for the 6, 8, and 10 orifices. These combinations of numbers and diameters aimed to keep the total cross-sectional area of orifices constant. The “inert” and the “combustible” conditions were chosen as MC atmosphere in this investigation.

Figure 9 shows the cone angle and the penetration under the “inert” condition with the three different numbers of orifices, and Fig. 10 exemplifies shadowgraph images corresponding to the condition.

Torch flame penetration showed little difference until about 2 ms ASOE in all cases, but the growth gradient for the 10-orifice case became slower around the timing, and the 6-orifice case showed a similar behavior at about 6 ms ASOE. The penetration becomes proportional to the square root of time after its growth becomes slower. This trend could be attributed to the difference in the momentum possessed by the individual torch flames. The larger the number of orifices is, the smaller the momentum of each torch flame is, and the earlier the penetration growth slows down. It suggests that the preceding unburned PC mixture could support the torch flame penetration according to the amount of the unburned mixture before slowing down claimed by Zhou et al. [23].

In contrast, the cone angle does not differ significantly depending on the number of orifices and increases slightly with the progress of the torch flame for any number of orifices. The boundary of the 6-orifice torch flame is more apparent than that of other torch flames. Whereas the bound-

aries of the 8 and 10-orifice cases are dimmer, especially around the tip of the torch flame. These may reflect the allocation of the energy possessed by the PC to each torch flame becomes larger for smaller orifice numbers.

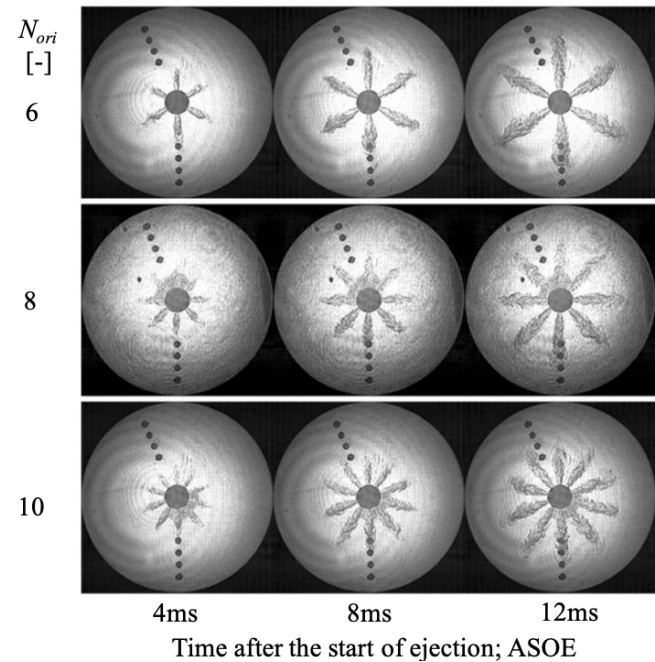


Fig. 10. Shadowgraphs of the different number of orifices ($N_{ori} = 6, 8, 10$) under “inert” condition

Figure 11 shows the effect of the number of orifices on the penetration and cone angle under “combustible” conditions.

Figure 12 shows the example images of torch flame ejection behavior under the corresponding conditions. The less the number of orifices is, the greater the amount of unburned air-fuel mixture ejected from each orifice is. This can promote the following MC combustion and results in a longer torch flame penetration and a wider cone angle of torch flame than those of the “inert” case. As mentioned before, in the “inert” case, the torch flames showed complicated behavior in the aspect of penetration due to the effects of the preceding unburned gas. However, in the “combustible” case, the preceding un-burned gas was quickly ignited by the torch flame, so the penetration changed according to the initial momentum of the torch flame. The torch flame in the 10-orifices case accelerates from the late stage of the penetration.

In contrast with the slight expansion of the cone angle over time in the “inert” conditions, the cone angle of torch flame under “combustible” conditions increases monotonically regardless of N_{ori} . This increase can be attributed to the combustion of the MC mixture. Especially when $N_{ori} = 6$, the torch flame expands more rapidly than the other two. Its slowest increase in cone angle can also explain the suppression of combustion in the case of $N_{ori} = 8$. From the observation results shown in Fig. 9, the torch flame has almost reached the combustion chamber wall by 15 ms ASOE regardless of the number of orifices. By the time of 10 ms ASOE shown in Fig. 9, some of the flame contours of $N_{ori} = 6$

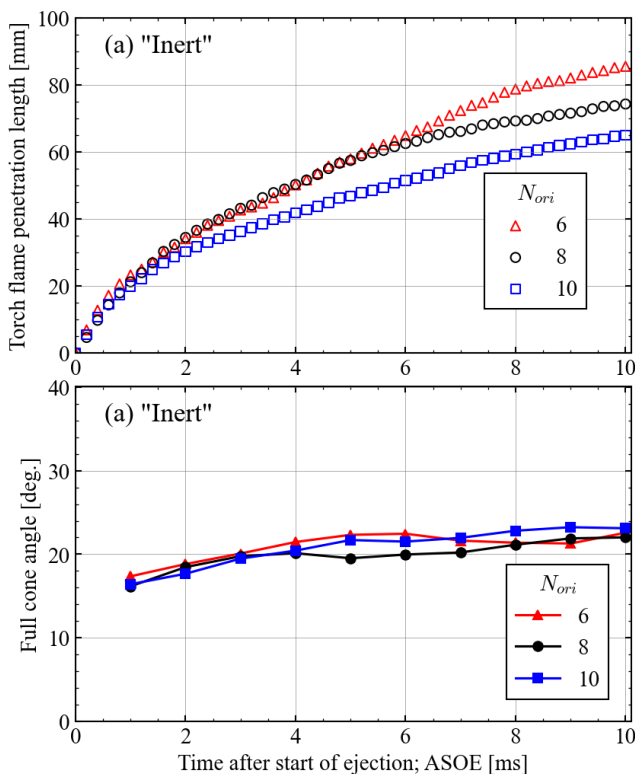


Fig. 9. Time history of (a) penetration, and (b) cone angle of the different number of orifices ($N_{ori} = 6, 8, 10$) under “inert” conditions

and 10 became horseshoe-shaped because the flames grew large enough to touch the bottom surface of the combustion chamber.

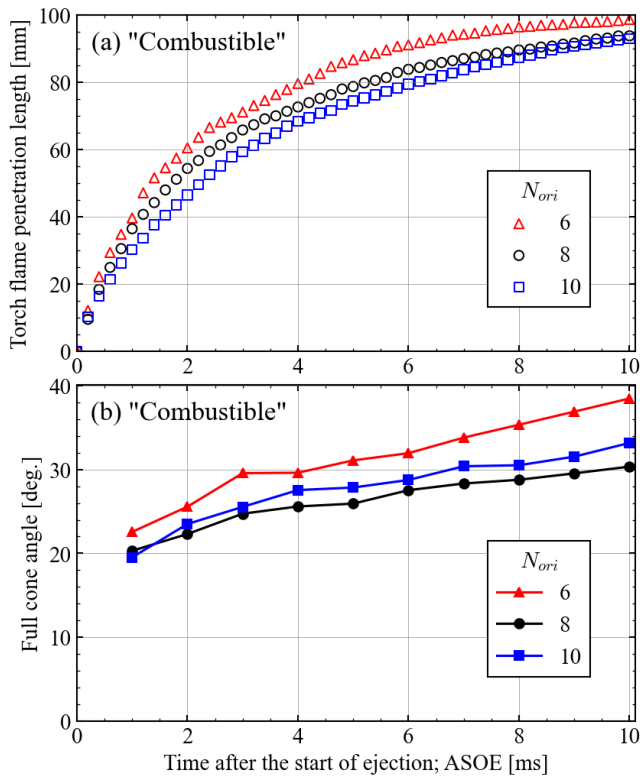


Fig. 11. Time history of (a) penetration, and (b) cone angle of the different number of orifices ($N_{ori} = 6, 8, 10$) under "combustible" conditions

In $N_{ori} = 8$, however, most of the torch flames were not flattened at 10 ms ASOE. This is consistent with the slowest growth of the cone angle of $N_{ori} = 8$ in Fig. 8. Thus, the

heat releasing process after 15 ms ASOE is mainly influenced by the flame propagation perpendicular to the orifice axis, that is, into the unburned MC mixture between two adjacent torch flames.

In $N_{ori} = 10$ at 10 ms ASOE, the torch flames begin to connect with each other. By 20 ms ASOE, they formed a united flame front with an undulating surface corresponding to the number of orifices. Compared to the other two cases,

$N_{ori} = 10$ case seemed to burn the entire MC mixture including the vicinity around the PC thanks to the connection.

Figure 13 shows the time history of the rate of heat release (ROHR) and the total amount of heat release based on the MC pressure. The rate of heat release is calculated from the measured pressure in MC using eq. (1) where Q is apparent heat release (heat release from combustion minus heat losses) and V is the volume of MC. The specific heat ratio κ is calculated based on the averaged MC gas composition and bulk mean MC temperature.

$$\frac{dQ}{dt} = \frac{V}{\kappa - 1} \frac{dP}{dt} \quad (1)$$

The time axis is ASOI (time after the start of ignition); for $N_{ori} = 6$ and $N_{ori} = 10$ cases, almost 12 ms ASOI, and for $N_{ori} = 8$ case, almost 14ms ASOI corresponds to 0 ms ASOE. As mentioned above, the torch flame reaches the MC wall at 15 ms ASOE. In $N_{ori} = 6$ and 10, around 15 ms ASOE corresponds to the time of the maximum heat release rate. In $N_{ori} = 8$, the timing was delayed. This is because $N_{ori} = 8$ case lags behind other N_{ori} cases in the development of combustion to the radial direction of the torch flame.

Here, we introduce an index named t_{40} . The t_{40} describes the time at which 40% of the heat from combustion has been released. The time base of t_{40} is also set to ASOI.

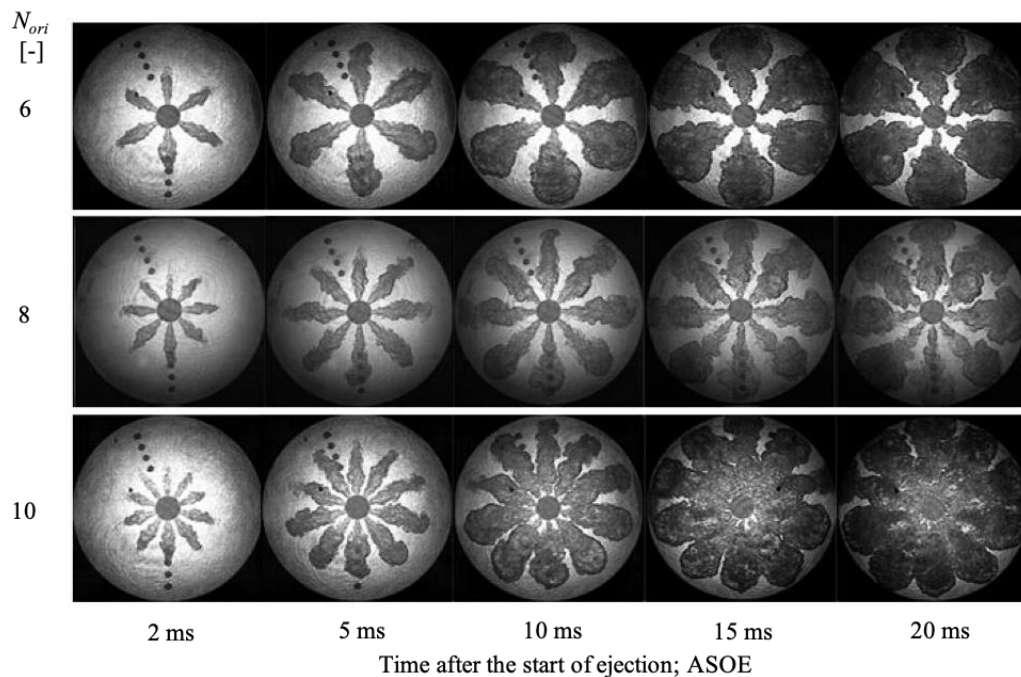


Fig. 12. Shadowgraph images of the different number of orifices ($N_{ori} = 6, 8, 10$) under "combustible" conditions

The t_{40} indicates the timing of the combustion end since the heat loss to the cold chamber wall would be dominant in the case of the CVCC and 40% of input heat was a good measure to estimate the maximum of released heat. When N_{ori} is 6, 8, and 10, t_{40} is 131 ms, 88.3 ms, and 78.2 ms, respectively. The t_{40} shows that the case with $N_{ori} = 10$ has the shortest combustion duration.

The peak value of the heat release rate is the highest in $N_{ori} = 10$ case in which the torch flames merged. After the heat release rates peaked at around 30 ms ASOI, the combustion was completed at $t_{40} = 78.2$ ms in $N_{ori} = 10$. The peak of heat release rate in $N_{ori} = 8$ was the most delayed and gentle among the three N_{ori} cases. The heat release rate of $N_{ori} = 6$ case rose quickest to its peak, but the period until the t_{40} is significantly longer than the other cases.

Based on the results of combustion visualization and pressure analysis described above, the entire mixture in the MC tended to burn efficiently when the torch flames merged, as explained in $N_{ori} = 10$ case.

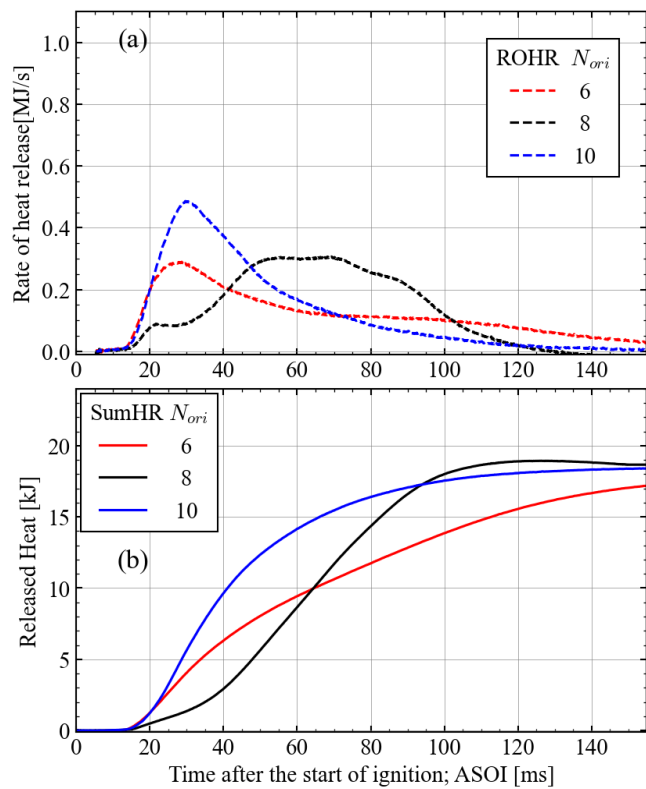


Fig. 13. Time history of (a) ROHR, and (b) of the different number of orifices ($N_{ori} = 6, 8, 10$) under “combustible” conditions

3.2. Effects of the orifice diameter

This section investigates the effect of orifice diameter change in the PC on the torch flame and MC mixture combustion. Since the number of orifices was constant at eight and the orifice diameters (D_{ori}) were set to 2.5 mm, 3.5 mm, 5.0 mm (tip ID #4, #1, #5), the ratio of the total cross-sectional area of these orifices was about 1: 2: 4.

Figure 14 shows the elapsed time history of the torch flame’s penetration length and cone angle when the MC was filled with “inert” ambient gas. Figure 15 shows the corresponding shadowgraph images of torch flames under the “inert” condition.

The penetration length increases with decreasing the orifice diameter, and this tendency has already appeared in the early stage of ejection. According to the momentum theory of a diesel spray [25], the penetration length of the spray varies in proportional to the square root of the orifice diameter.

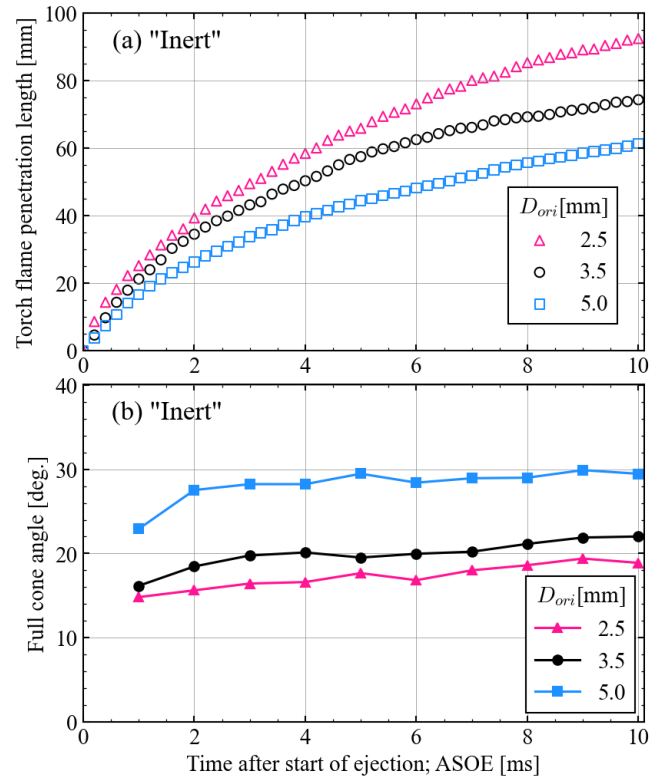


Fig. 14. Time history of (a) penetration, and (b) cone angle of different orifice diameter ($D_{ori} = 2.5, 3.5, 5.0$ mm) under “inert” condition

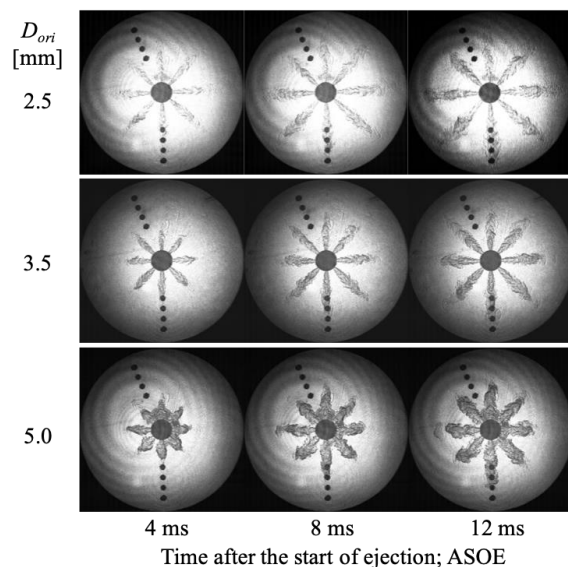


Fig. 15. Shadowgraphs of different orifice diameter ($D_{ori} = 2.5, 3.5, 5.0$ mm) under “inert” condition

The ratio of the square root of the orifice diameter is 1: 1.18: 1.41, and the ratio of the corresponding penetration length from the center of the PC is 76.6 mm (1): 89.4 mm

(1.17): 108.5 mm (1.42) at 15 ms ASOE, so the momentum theory seems to fit the torch flame as well. The cone angle is consistently larger for a larger orifice diameter.

For the smallest diameter case, $D_{ori} = 2.5$ mm, the torch flame boundary is unclear, and the flame tends to quench, especially near the exit of the PC orifice because the torch flames may be excessively stretched and cooled [19, 23] in the case of $D_{ori} = 2.5$ mm just after the ejection.

For $D_{ori} = 3.5$ mm, the unburned mixture can be observed to precede the tips of torch flames. The torch flame of $D_{ori} = 5.0$ mm clearly differs from the other orifices in the aspect of combustion, and the combustion continues even in the MC. For a $D_{ori} = 5$ mm, the cooling effect through the orifice would be reduced, and the torch flame would not be quenched. This implies that the orifice diameter greatly affects the ejection behavior of torch flames from the PC.

Figure 16 shows the effect of orifice diameter on the torch flame's penetration length and cone angle under "combustible" conditions. Figure 17 shows the corresponding shadowgraph images of torch flame ejection behavior under "combustible" conditions.

As explained, the penetration lengths in the "combustible" condition are longer than those in the "inert" condition. From the discussion in Section 3.1, this elongation of the penetration length can be attributed to the ignition of the unburned mixture volume attached to the torch flame tip and the combustion continuing in the MC mixture. The tendency for smaller orifice diameters to result in longer penetration length remains unchanged under combustible conditions.

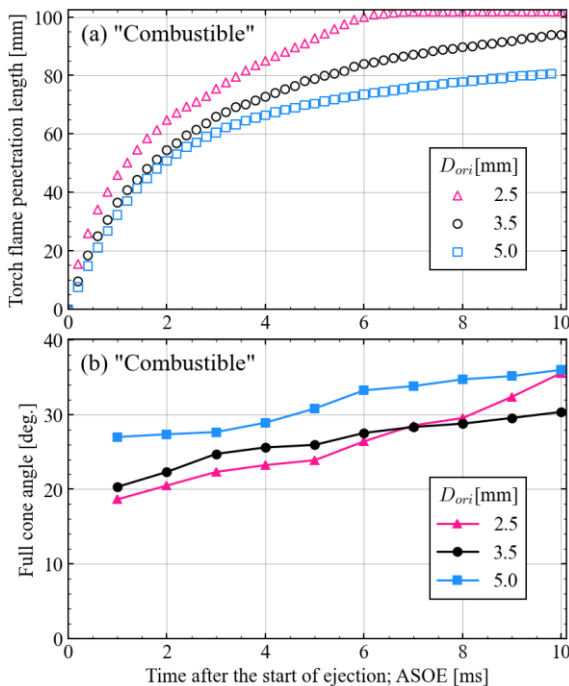


Fig. 16. Time history of (a) penetration, and (b) cone angle of different orifice diameter ($D_{ori} = 2.5, 3.5, 5.0$ mm) under "combustible" condition

In particular, the torch flame from $D_{ori} = 2.5$ mm impinged on the chamber wall at as early as 6 ms ASOE. Unlike the "inert" condition, the cone angle increased with

time, and the increasing gradient was more evident in $D_{ori} = 2.5$ mm than in other orifice diameters. In $D_{ori} = 2.5$ mm case, the combustion process is inferred to be different from others.

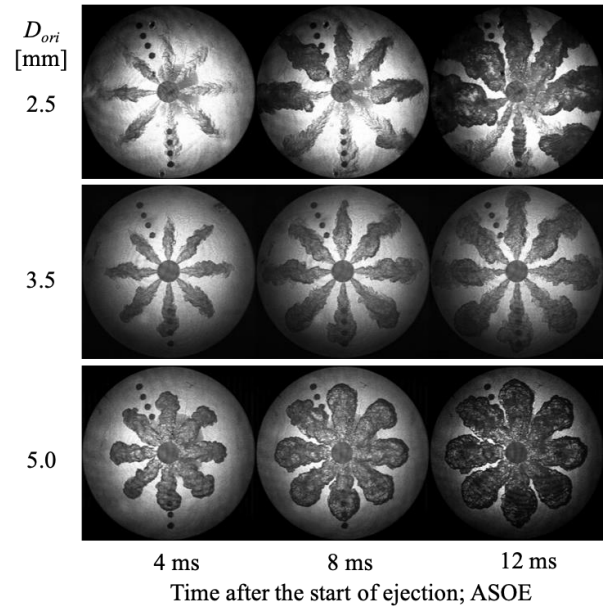


Fig. 17. Shadowgraphs of different orifice diameter ($D_{ori} = 2.5, 3.5, 5.0$ mm) under "combustible" condition

From the shadowgraph images in Fig. 17, the ignition process of MC mixture by the PC torch flames can be discussed in detail. In the case of $D_{ori} = 2.5$ mm at 4 ms ASOE, half of the torch flames could not ignite the MC mixture, and their ignition delay would be longer than 4 ms ASOE. At 8 ms ASOE, most of the torch flame ignited the MC mixture around the tip of the torch flames, but the torch jets still failed to ignite around their base. Finally, all the torch flames ignited the mixture at 12 ms ASOE, but the MC mixture flames could not go up to the orifice because of the excessive ejection velocity of the torch. Consequently, the combustion variation among the torch flames was evident when the orifice diameter was too small.

The torch flame of $D_{ori} = 3.5$ mm has already ignited the MC mixture at 4ms ASOE, but its tip is still thin at this timing. In the 12 ms ASOE, the tip of the torch flame expanded, but the MC mixture between two adjacent torch flames remained unburned.

In contrast, the torch flame of $D_{ori} = 5.0$ mm already ignited the MC mixture before 4 ms ASOE, and the tip of the torch flame is swelling like a snakehead. The torch flames merged in the vicinity of the PC and succeeded in consuming the mixture between the torch flames efficiently.

Figure 18 shows the difference in the history of the heat release rate and total heat release amount based on the MC pressure depending on the diameter of the orifice. The time axis is ASOI, and approximately 13 ms ASOI corresponds to ASOE for all orifice diameters.

The t_{40} , which is used as an index of the combustion end timing in the tested CVCC, was NA (combustion was too slow to reach 40% level), 88.3 ms, and 38.5 ms for $D_{ori} = 2.5, 3.5,$ and 5.0 mm, respectively.

In $D_{ori} = 2.5$ mm, which showed a very non-uniform combustion pattern, the maximum value of heat release rate was the smallest, and the period of heat release was excessively extended as explained above. However, this $D_{ori} = 2.5$ mm case has the shortest period before the heat release rate reaches its maximum value. On the other hand, for $D_{ori} = 5.0$ mm, the maximum heat release rate is at least three times higher than in the other cases. The peak value was the highest among all the orifices used in this experiment. In addition, the heat release rate rose rapidly, and the heat release ended quickly after its peak.

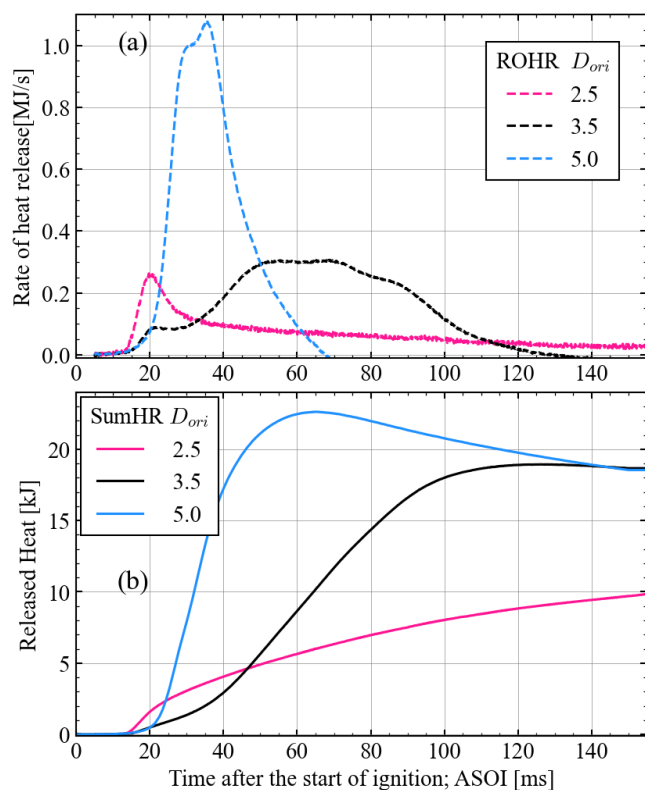


Fig. 18. Time history of (a) ROHR, and (b) of different orifice diameter ($D_{ori} = 2.5, 3.5, 5.0$ mm) under "combustible" condition

Thus, in the CVCC experiments under the initial condition at room temperature, it can be seen that the orifice diameter has significant effects both on the torch flame ejection behavior and the following MC combustion. Excessively small orifice diameter resulted in excessive ejection velocity and deterioration of ignition possibility of a torch flame. This result is in agreement with the experimental results of a PC-type small gas engine [26].

Contrariwise, larger orifice diameter resulted in slower torch ejection, but the combustion speed could be significantly accelerated when the torch flames were thick enough to merge near the exit of PC orifices. Therefore, it seems to be important for PC-type gas engines to promote combustion in the area between the torch flames by optimizing PC tip configuration.

4. Conclusions

This study investigates the effects of the PC configurations on torch flame propagation and MC combustion. The number and the diameter of the orifices were chosen as

parameters to investigate. Combustion visualization and pressure analysis were performed using a constant volume combustion chamber, which simulates the combustion chamber of a medium-speed pre-chamber type gas engine used in marine and industrial applications. The results can be summarized as follows:

The potential of PC for ejecting effective torch flames was objectively examined by changing the MC ambient gas from nitrogen, and artificial air, to lean CH_4/air mixture. With nitrogen filled in MC, the "inert" case named in this paper, the pure momentum of torch flame ejected from PC can be evaluated, whereas the torch flame combustion can continue with the latter two MC ambient gases. The flame propagation from torch flames can be detected with the mixture ambient which is named the "combustible" case. The "inert" MC gas showed the shortest penetration because the unburned mixture on the tip of the torch flame is diluted by the nitrogen, but the other two ambient gases showed about the same penetration. This implies torch flame penetration is determined only by the sustainability of combustion reactions instead of the combustibility of the MC gas.

Contrarily, the cone angle of the torch flame varies significantly depending on the combustibility of the MC gas. In both the "inert" and the artificial air cases, the cone angle remained constant, but the cone angle in the "combustible" case was consistently more extensive and increased monotonically with time. Flame propagation of the MC mixture in a PC-type gas engine appears as radial growth perpendicular to the axis of the torch flame, rather than in the axial direction.

The effects of the number of orifices; N_{ori} were investigated by keeping the total opening area of orifices constant. In the "inert" cases, a small number of orifices was advantageous for getting longer penetration, but N_{ori} hardly affects the cone angle of the torch flame. As for the penetrating behavior of torch flame irrespective of N_{ori} , the initial penetration proceeds at a certain distance in proportion to time, and the penetration becomes proportional to the square root of time after the torch flame is fully developed. This behavior is similar to that of a steady gas jet.

Torch flame and MC combustion behavior were observed under "combustible" conditions in the MC. Penetration gets longer than the "inert" condition regardless of N_{ori} , and increases as N_{ori} decreases. However, the preceding unburned gas was quickly ignited by the torch flame, so the penetration changed according to the initial momentum of the torch flame. On the contrary, cone angle increases with flame growth. When N_{ori} is small, the initial growth of the torch flame is faster, but the premixed gases between the torch flames take a longer time to burn because of the wider spacing between the torch flames. Based on observations of heat release rates and visualization images, an important factor for PC-type premixed gas engines is to promote combustion of the premixed gas between the torch flames. With small N_{ori} , both penetration and cone angle increase due to the increased momentum of individual torch flames, but the combustion of the premixed air between torch flames is not necessarily promoted. When the optimum number of orifices is selected, the torch flames come into

contact with each other in the early stage of combustion and grow toward the chamber wall as an apparently unified turbulent flame, resulting in faster combustion.

The effects of orifice diameter; D_{ori} were also investigated. Under "inert" conditions in the MC, the ratio of the square root of D_{ori} to the ratio of the penetration is in good agreement. Thus, the torch flame can be regarded as a steady gas jet, and the momentum theory of the spray can be applied to torch flames. The cone angle is consistently larger for larger D_{ori} . Excessively high jet velocity at small D_{ori} increases flame stretching and cooling losses at the orifice hole.

Under "combustible" conditions, the penetration is consistently larger than in the "inert" cases, but smaller D_{ori} results in longer penetration as well as in the "inert" case.

The cone angle trend is related to the ignitability of the torch flame to the MC premixture. When the jetting velocity of the torch flame is excessive, the ignition delay is also elongated, and after ignition, it is rapidly expanded by the entrained MC premixture. For this reason, the smaller D_{ori} , the greater the rate of increase in cone angle. For a small D_{ori} , the rate of heat generation is faster at the onset and at the first peak, but the subsequent combustion is slower. When D_{ori} is large, the start-up is slightly slower, but the flame propagates into the premixed air between the torch flames, and the total heat generation increases. When D_{ori} increases to a certain degree and the torch flames come into contact in the early stage of combustion, faster combustion as described above is achieved.

Nomenclature

A_{ori}	total area of pre-chamber orifice	MC	main chamber
ASOE	after the start of ejection	N_{ori}	the number of pre-chamber orifice
ASOI	after the start of ignition	NO_x	nitrogen oxide
CFD	computational fluid dynamics	N_2	nitrogen
CH_4	methane	O_2	oxygen
CVCC	constant volume combustion chamber	PC	pre-chamber
D	diameter	PM	particulate matter
D_{tip}	inner diameter of pre-chamber tip	RCM	rapid compression machine
D_{ori}	diameter of pre-chamber orifice	SO_x	sulfur oxide emissions
FMDF	filtered mass density function	t	thickness
GHG	greenhouse gas	TJI	turbulent jet ignition
H	high	V_{MC}	volume of main chamber
LES	large eddy simulation	V_{PC}	volume of pre-chamber
LIF	laser-induced fluorescence	λ	global air excess ratio
L_{ori}	length of pre-chamber orifice		

Bibliography

- [1] AL-ENAZI, A., OKONKWO, E.C., BICER, Y. et al. A review of cleaner alternative fuels for maritime transportation. *Energy Reports*. 2021, **7**, 1962-1985. <https://doi.org/10.1016/j.egy.2021.03.036>
- [2] LIU, J., ULISHNEY, C.J., DUMITRESCU, C.E. Experimental investigation of a heavy-duty natural gas engine performance operated at stoichiometric and lean operations. *Energy Conversion and Management*. 2021, **243**, 114401. <https://doi.org/10.1016/j.enconman.2021.114401>
- [3] KHAN, M.I., YASMIN, T., SHAKOOR, A. Technical overview of compressed natural gas (CNG) as a transportation fuel. *Renewable and Sustainable Energy Reviews*. 2015, **51**, 785-797. <https://doi.org/10.1016/j.rser.2015.06.053>
- [4] CHO, H.M., HE, B.Q. Spark ignition natural gas engines – a review. *Energy Conversion and Management*. 2007, **48**(2), 608-618. <https://doi.org/10.1016/j.enconman.2006.05.023>
- [5] EINEWALL, P., JOHANSSON, B. Cylinder to cylinder and cycle to cycle variations in a six cylinder lean burn natural gas engine. *SAE Technical Papers* 2000-01-1941. <https://doi.org/10.4271/2000-01-1941>
- [6] DUAN, X., DENG, B., LIU, Y. et al. An experimental study the impact of the hydrogen enrichment on cycle-to-cycle variations of the large bore and lean burn natural gas spark-ignition engine. *Fuel*. 2020, **282**, 118868. <https://doi.org/10.1016/j.fuel.2020.118868>
- [7] DALE, J.D., CHECKEL, M.D., SMY, P.R. Application of high energy ignition systems to engines. *Progress in Energy and Combustion Science*. 1997, **23**(5-6), 379-398. [https://doi.org/10.1016/S0360-1285\(97\)00011-7](https://doi.org/10.1016/S0360-1285(97)00011-7)
- [8] STARIKOVSKIY, A., ALEKSANDROV, N. Plasma-assisted ignition and combustion. *Progress in Energy and Combustion Science*. 2013, **39**(1), 61-110. <https://doi.org/10.1016/j.peccs.2012.05.003>
- [9] BAK, M.S., DO, H., MUNGAL, M.G. et al. Plasma-assisted stabilization of laminar premixed methane/air flames around the lean flammability limit. *Combustion and Flame*. 2012, **159**(10), 3128-3137. <https://doi.org/10.1016/j.combustflame.2012.03.023>
- [10] WERMER, L., LEFKOWITZ, J.K., OMBRELLO, T. et al. Spark and flame kernel interaction with dual-pulse laser-induced spark ignition in a lean premixed methane–air flow. *Energy*. 2021, **215**, 119162. <https://doi.org/10.1016/j.energy.2020.119162>
- [11] BUESCHKE, W., SZWAJCA, F., WISLOCKI, K. Experimental study on ignitability of lean cng/air mixture in the multi-stage cascade engine combustion system. *SAE Technical Papers* 2020-01-2084. 2020. <https://doi.org/10.4271/2020-01-2084>
- [12] GHORBANI, A., STEINHILBER, G., MARKUS, D. et al. Ignition by transient hot turbulent jets: An investigation of ignition mechanisms by means of a PDF/REDIM method.

- Proceedings of the Combustion Institute*. 2015, **35**(2), 2191-2198. <https://doi.org/10.1016/j.proci.2014.06.104>
- [13] ATTARD, W.P., FRASER, N., PARSONS, P. et al. A Turbulent Jet Ignition pre-chamber combustion system for large fuel economy improvements in a modern vehicle powertrain. *SAE International Journal of Engines*. 2010, **3**(2), 20-37. <https://doi.org/10.4271/2010-01-1457>
- [14] ATTARD, W.P., KOHN, J., PARSONS, P. Ignition energy development for a spark initiated combustion system capable of high load, high efficiency and near zero NO_x emissions. *SAE International Journal of Engines*. 2010, **3**(2), 481-496. <https://doi.org/10.4271/2010-32-0088>
- [15] ALVAREZ, C.E.C., COUTO, G.E., ROSO, V.R. et al. A review of prechamber ignition systems as lean combustion technology for SI engines. *Applied Thermal Engineering*. 2018, **128**, 107-120. <https://doi.org/10.1016/j.applthermaleng.2017.08.118>
- [16] ZHU, S., AKEHURST, S., LEWIS, A. et al. A review of the pre-chamber ignition system applied on future low-carbon spark ignition engines. *Renewable and Sustainable Energy Reviews*. 2022, **154**, 111872. <https://doi.org/10.1016/j.rser.2021.111872>
- [17] VALIDI, A.A., SCHOCK, H., JABERI, F. Turbulent jet ignition assisted combustion in a rapid compression machine. *Combustion and Flame*. 2017, **186**, 65-82. <https://doi.org/10.1016/j.combustflame.2017.07.032>
- [18] SADANANDAN, R., MARKUS, D., SCHIEßL, R. et al. Detailed investigation of ignition by hot gas jets. *Proceedings of the Combustion Institute*. 2007, **31**(1), 719-726. <https://doi.org/10.1016/j.proci.2006.08.027>
- [19] BISWAS, S., TANVIR, S., WANG, H. et al. On ignition mechanisms of premixed CH₄/air and H₂/air using a hot turbulent jet generated by pre-chamber combustion. *Applied Thermal Engineering*. 2016, **106**, 925-937. <https://doi.org/10.1016/j.applthermaleng.2016.06.070>
- [20] BUESCHKE, W., SKOWRON, M., SZWAJCA, F. et al. Flame propagation velocity in 2-stage gas combustion system applied in SI engine. *IOP Conference Series: Materials Science and Engineering*. 2018, **421**(4). <https://doi.org/10.1088/1757-899X/421/4/042009>
- [21] BUESCHKE, W., SKOWRON, M., WISŁOCKI, K. et al. Comparative study on combustion characteristics of lean premixed CH₄/air mixtures in RCM using spark ignition and turbulent jet ignition in terms of orifices angular position change. *Combustion Engines*. 2019, **176**(1), 36-41. <https://doi.org/10.19206/CE-2019-105>
- [22] GENTZ, G., GHOLAMISHEERI, M., TOULSON, E. A study of a turbulent jet ignition system fueled with iso-octane: pressure trace analysis and combustion visualization. *Applied Energy*. 2017, **189**, 385-394. <https://doi.org/10.1016/j.apenergy.2016.12.055>
- [23] ZHOU, L., SONG, Y., HUA, J. et al. Effects of different hole structures of pre-chamber with turbulent jet ignition on the flame propagation and lean combustion performance of a single-cylinder engine. *Fuel*. 2022, **308**, 121902. <https://doi.org/10.1016/j.fuel.2021.121902>
- [24] PIELECHA, I., BUESCHKE, W., SKOWRON, M. et al. Prechamber optimal selection for a two stage turbulent jet ignition type combustion system in CNG-fuelled engine. *Combustion Engines*. 2019, **176**(1), 16-26. <https://doi.org/10.19206/CE-2019-103>
- [25] WAKURI, Y., FUJII, M., AMITANI, T. et al. Studies on the penetration of fuel spray of diesel engine. *Transactions of the JSME*. 2015, **7**(11), 101-104. <https://doi.org/10.1299/kikai1938.25.820>
- [26] NAKANO, H., KAYA, R., KOBAYASHI, S. et al. A study on the influence of the strength of ejected jet on combustion in a natural gas lean burn engine with a sub-chamber with direct injector inside. *COMODIA 2017 – 9th International Conference on Modeling and Diagnostics for Advanced Engine Systems*. 2017. <https://doi.org/10.1299/jmsesdm.2017.9.c301>

Takuya Wakasugi, BEng. – Interdisciplinary Graduate School of Engineering Sciences, Kyushu University, Japan.

e-mail: wakasugi.takuya.875@s.kyushu-u.ac.jp



Hiroshi Tashima, DEng. – Faculty of Engineering Sciences, Kyushu University, Japan.

e-mail: tajima.hiroshi.539@m.kyushu-u.ac.jp



Daisuke Tsuru, DEng. – Faculty of Engineering Sciences, Kyushu University, Japan.

e-mail: dtsuru@ence.kyushu-u.ac.jp

